Microstructure, Mechanical Properties and Friction Behavior of Magnetron-sputtered V-C Coatings

Pantcho Stoyanov[1,2*], Johannes Schneider[1], Monika Rinke[1], Sven Ulrich[1], Eberhard Nold[2], Martin Dienwiebel[1,2] and Michael Stüber[1*]

[1] Karlsruhe Institute of Technology, Institute for Applied Materials (IAM),
Kaiserstraße 12, 76131 Karlsruhe, Germany

[2] Fraunhofer-Institute for Mechanics of Materials IWM
Wöhlerstrasse 11, 79108 Freiburg, Germany

*Corresponding authors:
michael.stueber@kit.edu,
pantcho.stoyanov@mail.mcgill.ca

Abstract:

This study links micro- to macroscale tribology in order to provide a better understanding of the sliding mechanisms of magnetron-sputtered vanadium carbide-based (V-C) coatings with varying microstructures (i.e. by varying the C/V concentration ratio systematically between 1 and 3). Correspondingly, volume fraction of the amorphous carbon phase increases with increasing the carbon content as shown by electron microprobe studies, X-ray diffraction and Raman spectroscopy; the thin films microstructure changes from single phase pure vanadium carbide films, f.c.c. VC_{1-x}, to nanocomposite films of nanocrystalline vanadium carbide and amorphous carbon phases, VC_{1-x}/a-C. Mechanical properties characterization shows that the indentation hardness (H) and the reduced modulus (E_r) of the coatings decrease with increasing the carbon concentration (i.e. H ranges between 15 and 33 GPa and E_r ranges between 239 and 391 GPa for the low and high vanadium concentration respectively). A similar behavior was also observed with the results on the critical load of failure obtained from scratch tests, where the coatings with the highest vanadium concentration exhibits higher critical load of failure and thus, better coating adhesion. However, reciprocating micro- and macroscale tribological tests

performed at a relative humidity level of 45±5% (i.e. normal load in the microtribological experiments is between 100 mN and 1 N and for the macroscale tribometry the normal load is 20 N) reveal higher friction values and increased wear with the high vanadium content coatings. This sliding behavior is attributed to differences in the third body formation (i.e. carbon based transfer- and tribo-film) and velocity accommodation modes, which are analyzed *ex situ* by means of X-ray photoelectron spectroscopy (XPS), micro-Raman spectroscopy and atomic force microscopy.

Keywords: vanadium carbide, carbon-based composites, non-reactive d.c. magnetron sputtering, microtribology, third bodies, velocity accommodation modes

1. Introduction

Tribological issues, such as friction and wear, are among the primary limiting factors for many metal-forming technologies and enabling components in drilling technologies, primarily due to the extreme operating conditions of these applications (i.e. large temperature fluctuations and high contact stresses). The development and implementation of materials capable of operating efficiently under these conditions has the potential to save metal-forming and drilling industries millions of dollars annually. For instance, abrasive wear, plastic deformation, chipping, adhesion, chemical instability, and thermal shock induced cracking are the main cause premature failure of tool components in warm/hot forging (e.g. shearing punch, valve forging die) (*1*-*3*). In addition, the mechanical properties of many currently used materials (e.g. high speed steels) degrade at high temperatures leading to a decrease in the endurance life. Similarly, in oil drilling applications, temperatures are well above 200˚C leading to premature failure of the cutting

materials. Replacement of the cutting tooth at these depths is nearly impossible and retracting the drill pipe for a repair is time consuming. Therefore, there is a strong desire in developing and implementing materials that not only can survive the harsh temperatures and pressures but are also capable of operating efficiently over billions of cycles.

Transition metal carbides exhibit superior mechanical and tribological properties at a wide range of environmental conditions and contact pressures (*4-10*) and thus, have received a lot of attention for the demanding application mentioned above. Indeed, tungsten carbide, typically bounded by Co with content ranging between 4 and 15 wt.% (*11*), is a common material used in demanding sliding conditions, and consequently has been studied intensely (*12-20*). In regards to the cutting tool applications, due to the complexity of velocity accommodation modes in tool-chip contacts (*11*), including plastic deformation and material transfer, and the need for multifunctional materials, a variety of advanced coatings have been considered with high abrasive wear resistance (e.g. high hardness), low surface adhesion (i.e. reduce material transfer), thermal and chemical stability, as well as low friction (i.e. minimize frictional heating) (*21-25*)(*26*). Such materials include pure carbon coatings in the form of amorphous carbon (a-C), amorphous hydrogenated carbon (a-C:H), tetrahedral amorphous carbon (ta-C, and ta-C:H), all of which have shown to attain low friction and high wear resistance (*27-33*). While these coatings seem promising at first, some drawbacks include internal stress issues as well as a decrease in tribological performance (i.e. high friction and low wear) at elevated temperatures (*27, 34*). In order to overcome such issues, there have been several research efforts directed towards metal doped DLC coatings, where typical metals consist of Cr, Cu, Ti, Ta, W, Nb and Zr (*35-37*). While research has focused signficantly towards TiC/a-C (*38-45*) and WC/a-C (*46-*

49), less literature can be found on combinations like CrC/a-C (*50, 51*), ZrC/a-C, NbC/a-C (*52*) or TaC/a-C (*53*).

More recently, vanadium based coatings have also been considered for a number of such applications (e.g. cutting tools, ball bearings, automotive components) due to their high corrosion resistance, radiation resistance, as well as mechanical stability at elevated temperatures (*36, 54-57*). Commonly, such coatings are deposited using physical vapor deposition (PVD) (*58, 59*), chemical vapor deposition (CVD) (*60*), Thermo-reactive Diffusion Treatment (TRD) (*61, 62*), laser cladding (*63*) and several other methods (*55, 64-69*). For instance, Wu et al. (*58*) investigated the microstructure and mechanical properties of vanadium carbide coatings deposited by reactive magnetron sputtering. By varying the C_2H_2 partial pressure, the authors demonstrated that vanadium carbide coatings can be synthesized using low partial pressures reaching peak hardness and elastic modulus at 35.5 GPa and 358 GPa respectively. Similarly, Aguzzoli et al. (*70*) studied the mechanical properties of vanadium carbide coatings deposited by DC reactive magnetron sputtering and found the peak hardness and resistance to plastic deformation (i.e. based on H^3/E^2 ratio (*71*)) to be for a carbon to vanadium (C/V) ratio of approximately 1.2. While these studies have provided significant new insights on deposition methods of vanadium carbides, the friction and wear mechanisms of these coatings have received little attention, in particular the tribological behavior of vanadium carbide/amorphous carbon nanocomposites.

In this study we investigate the influence of C/V ratio (i.e. from pure crystalline VC_{1-x} to nanocomposite VC_{1-x}/a-C thin films) on the microstructure, mechanical properties, and tribological behavior to assess their reliability and limitations. In addition, in this study we link

micro- to macroscale tribology in order to provide an excessive understanding of the sliding mechanisms of the various vanadium carbide-based (V-C) coatings.

2. Experimental Procedure

The coatings in this study are prepared using non-reactive d.c. magnetron sputtering (i.e. Leybold Z 550 PVD coater) with a symmetrically segmented VC/graphite target (i.e. target diameter of 75 mm with a 5 mm thickness, target-to-substrates distance approximately 5 cm, 500 W d.c. target power, argon gas pressure 0.6 Pa, grounded substrate, substrate temperature < 150 °C) on a commercial WC-Co substrate (with composition 70.5 at.% WC, 27.9 at.% Co, rest NbC and TaC, supplier: Walter AG, Germany), as shown in Figure 1. The targets were made out of half-circular plates of commercial vanadium carbide (Livermore, California, USA) and graphite (Schunk Kohlenstofftechnik, Germany), bonded onto a copper substrate holder. The pre-treatment of substrates includes mechanical polishing (i.e. mirror like surface, < 1 micron), ultrasonic bath in isopropanol, in vacuum r.f. plasma etching for 15 minutes in pure argon at 0.6 Pa, and - 800 V substrate bias to remove surface contamination and oxides. More details on this methodology is found elsewhere (*72*) . The approach in thin film design enables a systematic combinatorics: The composition of the coatings is varied by placing three substrates in a linier fashion relative to the segmented target, according to Figure 1. The experimental combinatorial approach to design such coatings is explained in (*73*) for another material system.. The resulting C:V ratios of the coatings vary between 1:1 and 1:3 (i.e. C/V = 1.2, 1.6, 2.9), resulting in V-C coatings with various microstructure (please see results section for details).

The elemental analysis is performed by means of X-ray photoelectron spectroscopy (PHI 5000 VersaProbe with AL Anode - Sputtering 1 kV Ar 500 nA 2x2 mm, sputter rate of 1.7

nm/min (SiO_2)) and electron probe microanalysis (EPMA; Camebax Microbeam). The microstructures of the as deposited coatings are characterized using X-ray diffraction (Bragg-Brentano mode, Seifert-Meteor using $Cu_{K\alpha}$-radiation) and cross-sectional focused ion beam (FIB) imaging (Zeiss-XB 1540). ~~while~~ More information on the constitution of the coatings is obtained from micro-Raman spectroscopy with a Renishaw 1000 Raman microscope. Raman scattering was excited by an argon laser at a wavelength of 514.5 nm (Modu-Laser Mod. Aries-163). At the sample spot of about 1 μm in diameter the maximum laser power of 2 - 3 mW was attenuated to 25% to avoid thermal dammage (graphitisation) of the sample. The spatial resolution of 1-2 μm was achieved with a ×50 Nplan objective. The spectral resolution of 1 cm^{-1} was achieved with a holographic grating with 2400 grooves mm^{-1}. The spectra were measured in the spectral range of 300-2000 cm^{-1} with a sampling time of 300 s using an UV-enhanced CCD detector operated at -70°C.). The hardness and reduced modulus of the coatings are evaluated by means of microindentation following the method described in (*74*) (using a CSM combi-platform type MCT-Z-AE, equipped with a Vickers shape diamond indenter). In addition, the critical loads of failure of the coatings in scratch testing is evaluated using a CSEM revetest using normal loads of 0-100N. The surface topography of the coatings was characterized by measuring the surface roughness average R_a, using a Tencor P10 surface profilometer.

Reciprocating sliding experiments are performed at the microscopic and macroscopic length scales under unlubricated conditions. The experiments are performed in ambient conditions (i.e. T = 20±2 °C and RH = 45±5 %). For the microtribology, a TETRA microtribometer is used, while the macro-scale sliding tests are performed using a (Optimol SRV II) tribometer. A Ruby sphere is used as a counterface for the microtribology tests with a radius of 0.5 mm and a Sapphire ball with a radius of 5 mm is used for the macroscale tribology. The

normal load in the microtribological experiments is varied between 100mN and 1N, while for the macroscale tribometry the normal load is 20 N in order to keep similar Hertzian contact pressures (i.e. between 1.5 and 2.2 GPa) for reliable comparison. The sliding speed for the microtribology tests was 0.05 mm/sec with wear tracks varying in length between 100 and 400 μm. In contrast, the wear track length of the macro-scale tribology tests was 2.5 mm and the frequency for the test was 20 Hz resulting in an average sliding speed of 100 mm/s. Ex situ analysis of the worn surfaces is performed by means of micro-Raman spectroscopy (system mentioned above), X-ray photoelectron spectroscopy, and Atomic Force Microscopy (i.e. for surface roughness measurements). The wear area was calculated and recorded from cross-sectional scans of the wear track.

3. Results

3.1 Coating Deposition and Microstructure

The coatings in this study are synthesized using non-reactive d.c. magnetron sputtering with a segmented VC/graphite target, as shown in Figure 1 (a). The coating composition is varied by placing the substrates in a linier fashion relative to the segmented target, resulting in V:C ratios vary between 1:1 and 1:3, as measured by means of EPMA. More specifically, the carbon concentration was measured 53at.%, 60at.%, and 72at.% for the different coatings. However, in this study we use the C/V ratio as the major descriptor of the coatings. It should be noted that, while we did not achieve perfect C/V = 1, the coatings in this study with highest V concentration are slightly above this perfect stoichiometry. Figure 1 (b) shows cross-sectional images of the various V-C coatings developed in this study, including atomic force microscope images of their surfaces. The cross-sectional images reveal more microscopic defects/voids with the high carbon

content coatings. Interestingly, the variation in the carbon content does not influence the surface roughness with all coatings having RMS of approximately 20 nm.

(a)

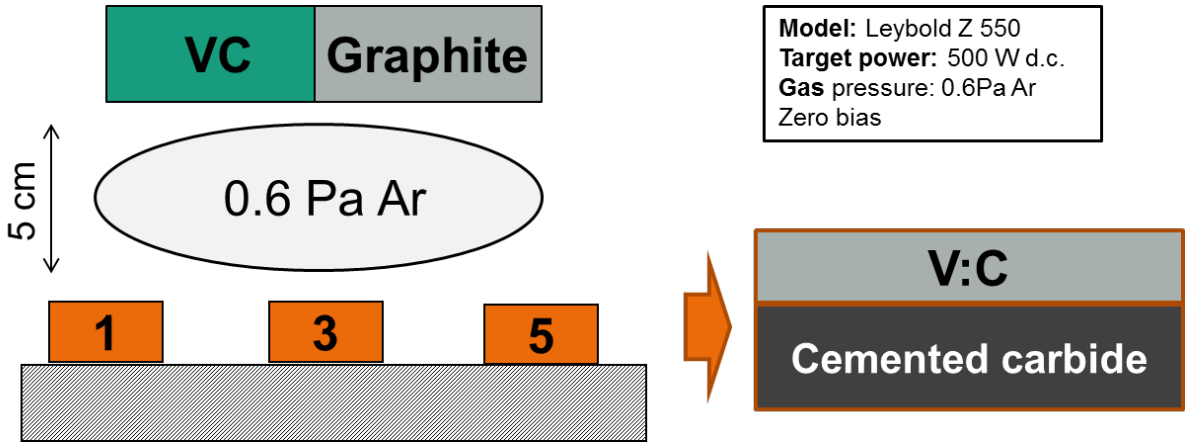

(b)

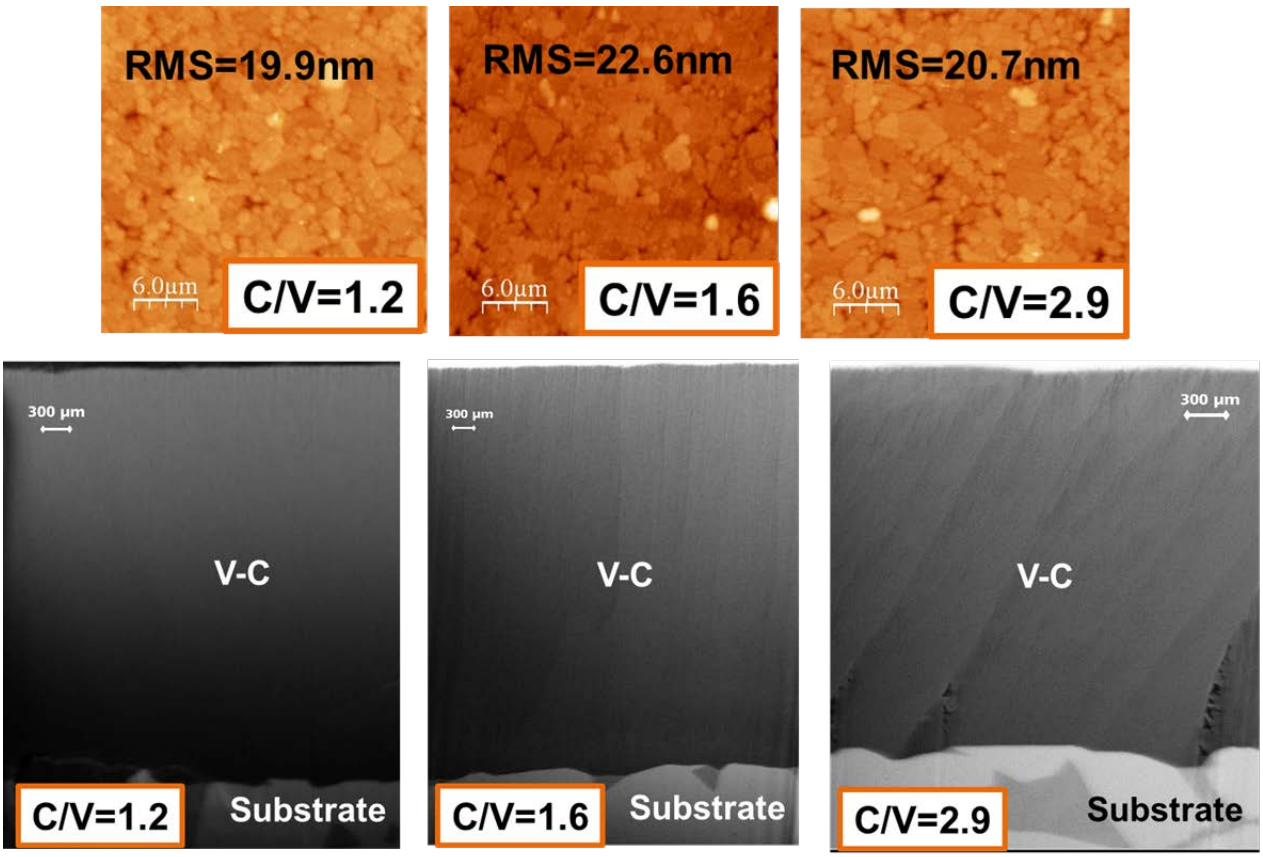

Figure 1 (a) Schematic representation of the non-reactive d.c. magnetron sputter deposition process used to develop the V-C coatings and **(b)** Cross-sectional SEM images of the vanadium cabide coatings including atomic force microscope images of the surface as subfigures.

X-ray photoelectron spectroscopy of the various coatings developed for this study (C/V = 1.2, 1.6, 2.9) is shown in Figure 2 as a function of the sputter depth. While a small oxide layer is observed on the surface of all coatings, the atomic oxygen concentration drops below 10% at 5 nm and below 5 % at 10 nm of sputtering depth. The atomic concentration of the carbon and vanadium correlate well with the results obtained with the electron probe micro analysis (EPMA). Subsequently to a 5 nm sputtering depth, the carbon and vanadium concentrations remain relatively constant with respect to the depth indicating an effective deposition process.

The concentration of carbon observed with the XPS is consistent with the micro-Raman spectra of the different coatings, as shown in Figure 3. The spectra of the C/V=2.9 coatings reveals apparent peaks at 1400 and 1570 cm^{-1} (i.e. values obtained from Gaussian fits) corresponding to D (disordered) and G (graphitic) peaks. While these peaks are also present with the lower carbon content coatings, the intensity is significantly lower and decreases with decreasing the carbon content. In addition, the ratio of the peak areas (I_D/I_G) decreases with increasing the carbon content for the unworn samples, as shown in table 1.

Table 1 Micro-Raman spectra of the different coatings in the worn and unworn state

C/V	Peak 1 /cm^{-1}	Peak D /cm^{-1}	Peak G/ cm^{-1}	Int 1	Int D	Int G	area 1	area D	area G	I_D/I_G area	ID/IG int_{max}
unworn											
1,17		1412	1588		150	94		55163	9842	5,60	1,60
1,56		1396	1571		268	170		92831	21899	4,24	1,58
2,87		1400	1570		629	420		223795	59801	3,74	1,50
Worn - macro											
1,17	927	1366	1564	101	286	211	16924	78973	29820	2,65	1,36
1,56	955	1378	1552	61	487	278	9307	149866	42567	3,52	1,75
2,87	954	1389	1564	113	2212	1395	15821	785083	193607	4,06	1,59

The microstructure of the coatings is investigated by means of X-ray diffraction and the results are shown in Figure 4. The high Vanadium content coatings reveal high intensity peaks of the (111) and (200) planes of Vanadium Carbide with an fcc structure. The other peaks in the spectrum correspond to the cemented carbide substrate. The XRD spectrum of this coating does not point to further phases except of the nanocrystalline f.c.c. VC phase. It should however be noted that the co-existence of an amorphous carbon phase in this coating cannot be completely excluded by referring to the XRD and Raman spectroscopy results. Nevertheless, this coating will be considered in this paper as single phase f.c.c. VC_{1+x} coating. While the vanadium carbide peaks are also present with the higher carbon content coatings, the intensity decreases significantly indicating a higher degree of amorphization (and/or a significant decrease in grain size) with increasing the carbon content. More specifically, the coatings with medium C/V concentration ratio (i.e. grown at the center positions of the target) seem to exhibit a large volume fraction of a f.c.c. vanadium carbide phase together with a larger volume fraction of an amorphous carbon phase (as is derived from the related Raman spectrum). Subsequently, the coatings with a high C/V concentration ratio (i.e. grown at the C-rich side of the target) exhibit a

significantly smaller volume fraction of a crystalline VC phase and a large volume fraction of an amorphous carbon phase. In summary, the structure of the coatings is varied from single-phase f.c.c. VC_{1+x} to nanocomposite VC/a-C with increasing C/V ratio. More detailed analysis will be performed by means of transmission electron microscopy (TEM) in order to elucidate on the structure of these coatings and will be presented in a future study.

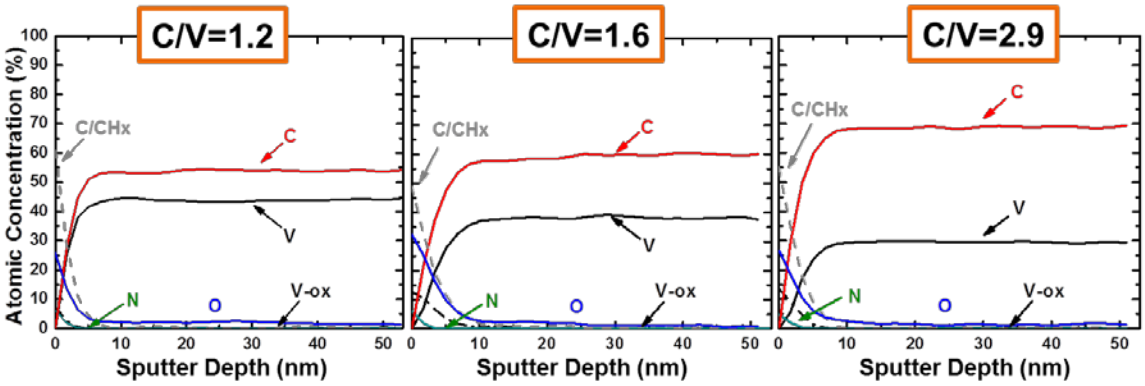

Figure 2 The atomic concentration vs. the sputter depth obtained by means of XPS revealing constant concentration with respect to the coatings thickness.

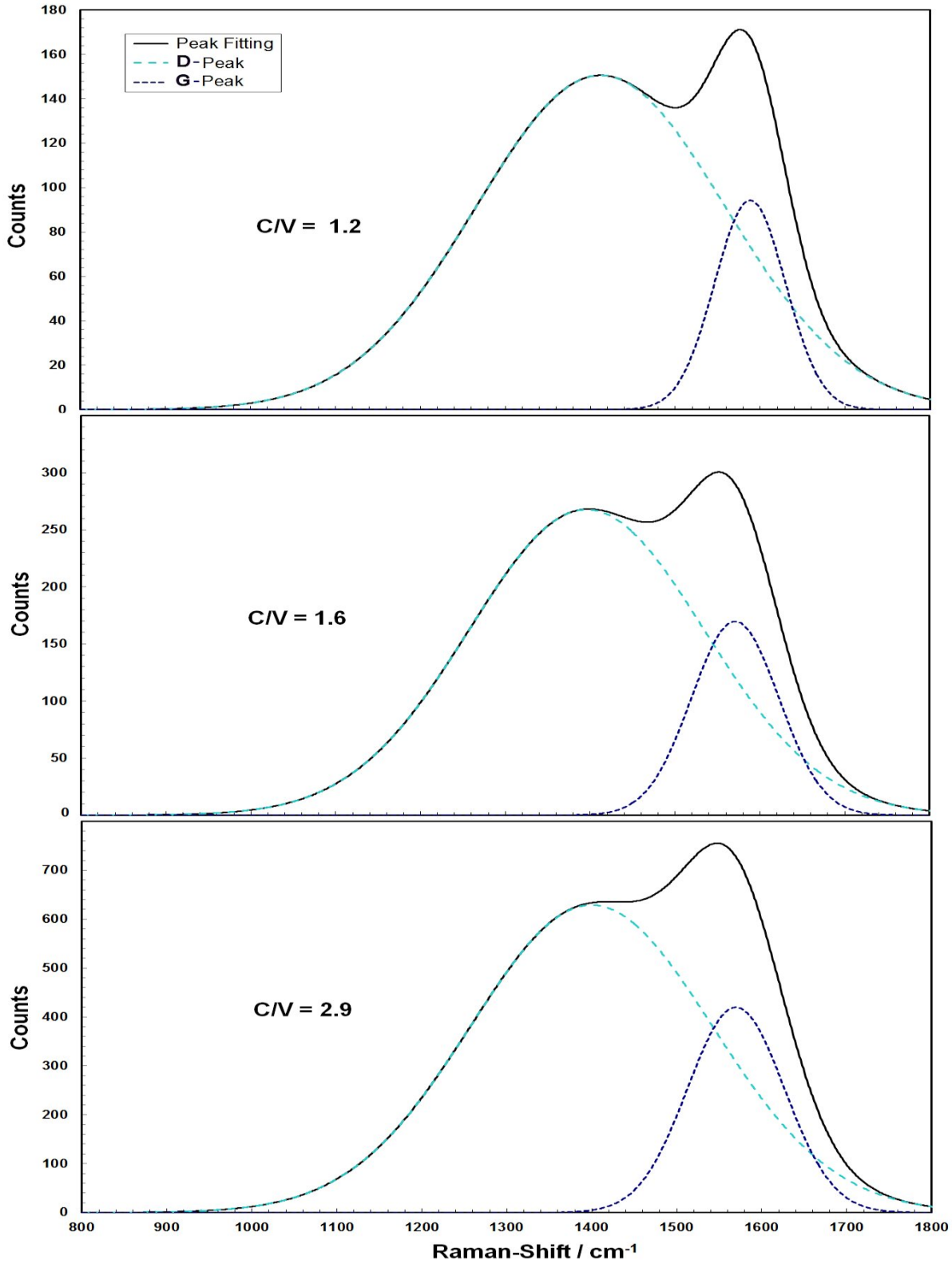

Figure 3 Micro-Raman analysis of the unworn surfaces for the various coatings revealing the increased intensity of the D- and G- band with increasing the carbon content.

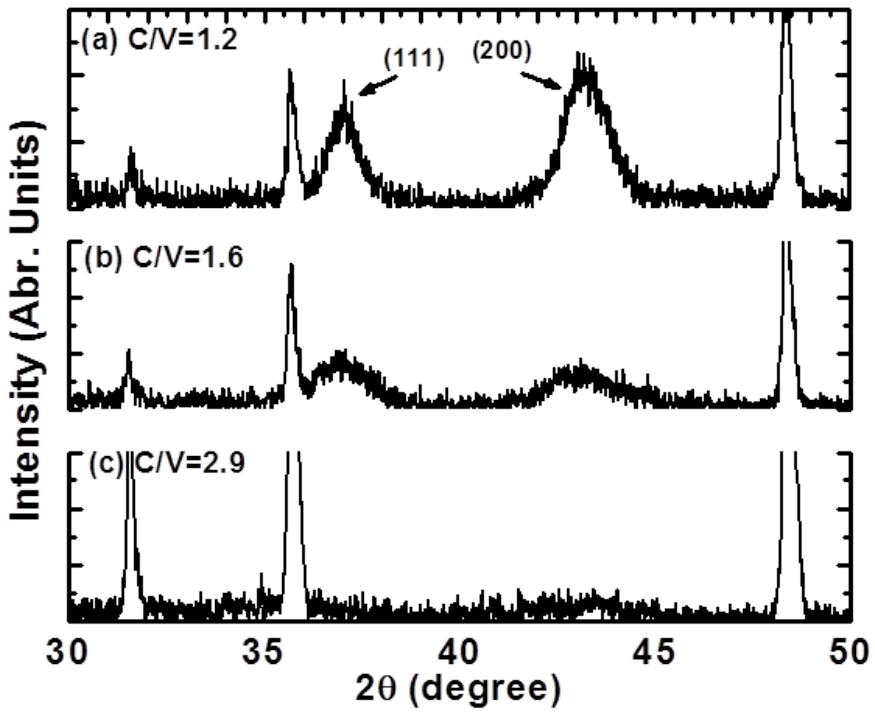

Figure 4 XRD analysis of the different as-deposited coatings showing the increase in the degree of amorphization with the higher carbon content coatings.

3.2 Mechanical Properties and Tribological Behavior

3.2.1 Mechanical Properties

The mechanical properties (i.e. Hardness and Reduced Modulus) of the coatings are evaluated by means of micro-indentation and are shown in Figure 5 vs. the C/V ratio. Noticeably, the hardness decreases from 33 GPa for single phase f.c.c. VC_{1+x} coatings with increasing the carbon content to approximately 17 GPa for the C/V=2.9 coating. The Reduced Modulus follows the trend of the hardness closely. This behavior of the hardness and reduced modulus is consistent with previous studies of similar vanadium carbide coatings (*58*).

Figure 5 (b) shows the H^3/Er^2 ratio and the critical load of failure L_{C1} (i.e. measured with a scratch testing apparatus) plotted vs. the C/V ratio. Similarly, to the hardness and reduced

modulus in Figure 5 (a), the H^3/Er^2 decreases with higher C/V ratio. The critical load follows this trend closely; the highest scratch resistance is observed with the lowest carbon content, while the lowest scratch resistance is observed with the lowest vanadium content coating.

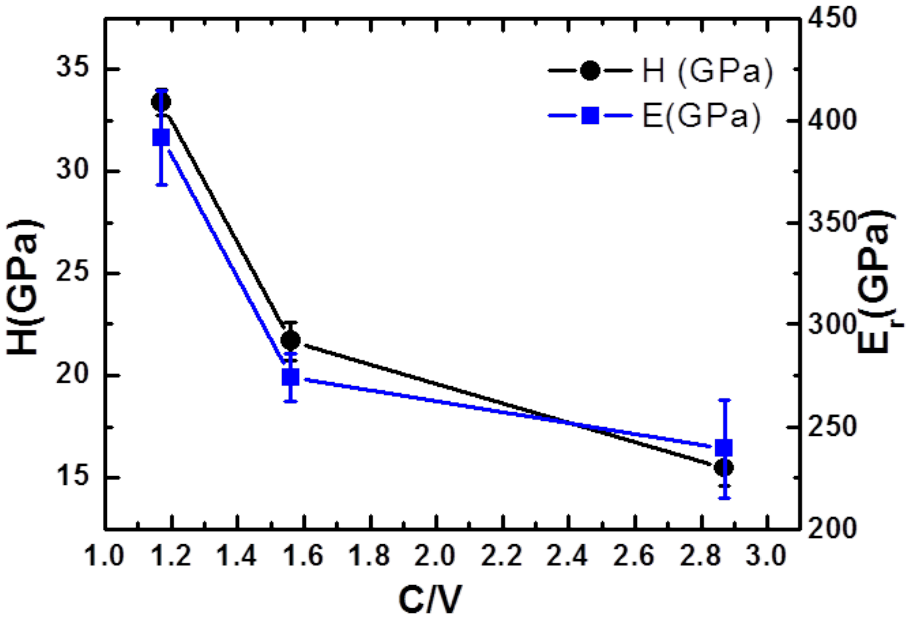

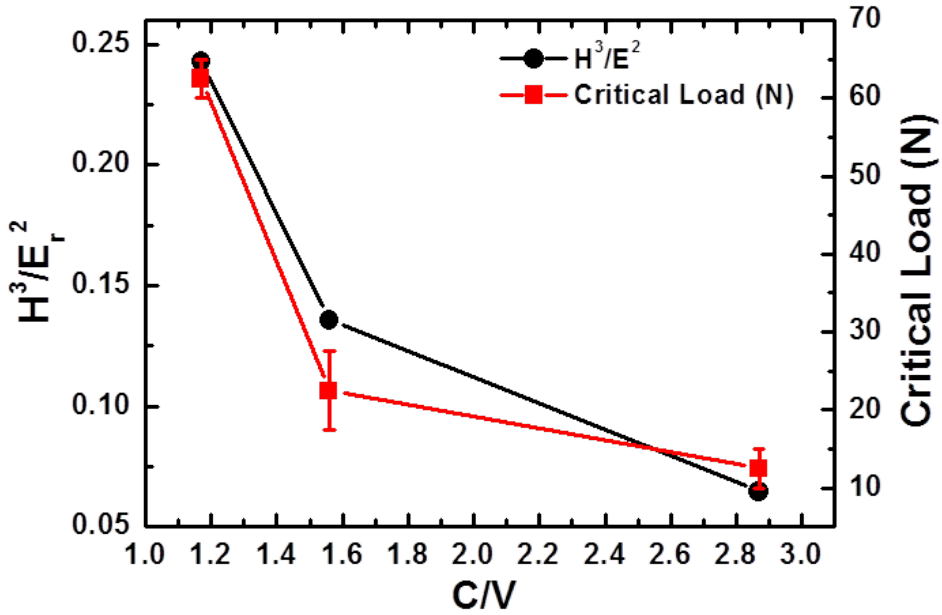

Figure 5(a) Hardness H and Reduced Modulus E_r vs. C/V and **(b)** H^3/Er^2 and Critical Load vs. C/V

3.2.2 Micro-scale Sliding Experiments

Micro-scale sliding experiments are performed on the vanadium carbide based coatings and the friction force (i.e. average values of steady state sliding) vs. the normal load is shown in Figure 6 (a). While the friction force increases nearly linearly for all coatings, the slopes are somewhat different; the lowest slope is 0.11 for the highest C/V ratio and 0.15 for the lowest C/V ratio. The slope is proportional to the coefficient of friction and thus, the microtribology results indicate a decrease in the friction coefficient with increase the carbon content. The surface adhesion, calculated using these results, is opposite to the friction behavior; the increase in carbon content increases the adhesion force (i.e. 7, 10, and 29 mN for the C/V=1.2, 1.6, and 2.9, respectively).

In order to observe the evolution of the friction, the coefficient of friction is plotted vs. the number of cycles in Figure 6 (b) for a normal load of 1000 mN. Initially, the friction coefficient is relatively similar for the three coatings. Subsequently, the friction coefficient of the highest vanadium content coating, i.e. the single phase f.c.c. VC_{1+x} coating, increases at a relatively high rate up to 0.2 after which it continuously increases at a slower rate, never reaching steady state sliding. The lowest carbon content coating, a VC/a-c nanocomposite coating, on the other hand, remains at approximately 0.125 with some fluctuations for the remainder of the experiment. Clearly, the coefficient of friction at steady state decreases with increasing the normal load.

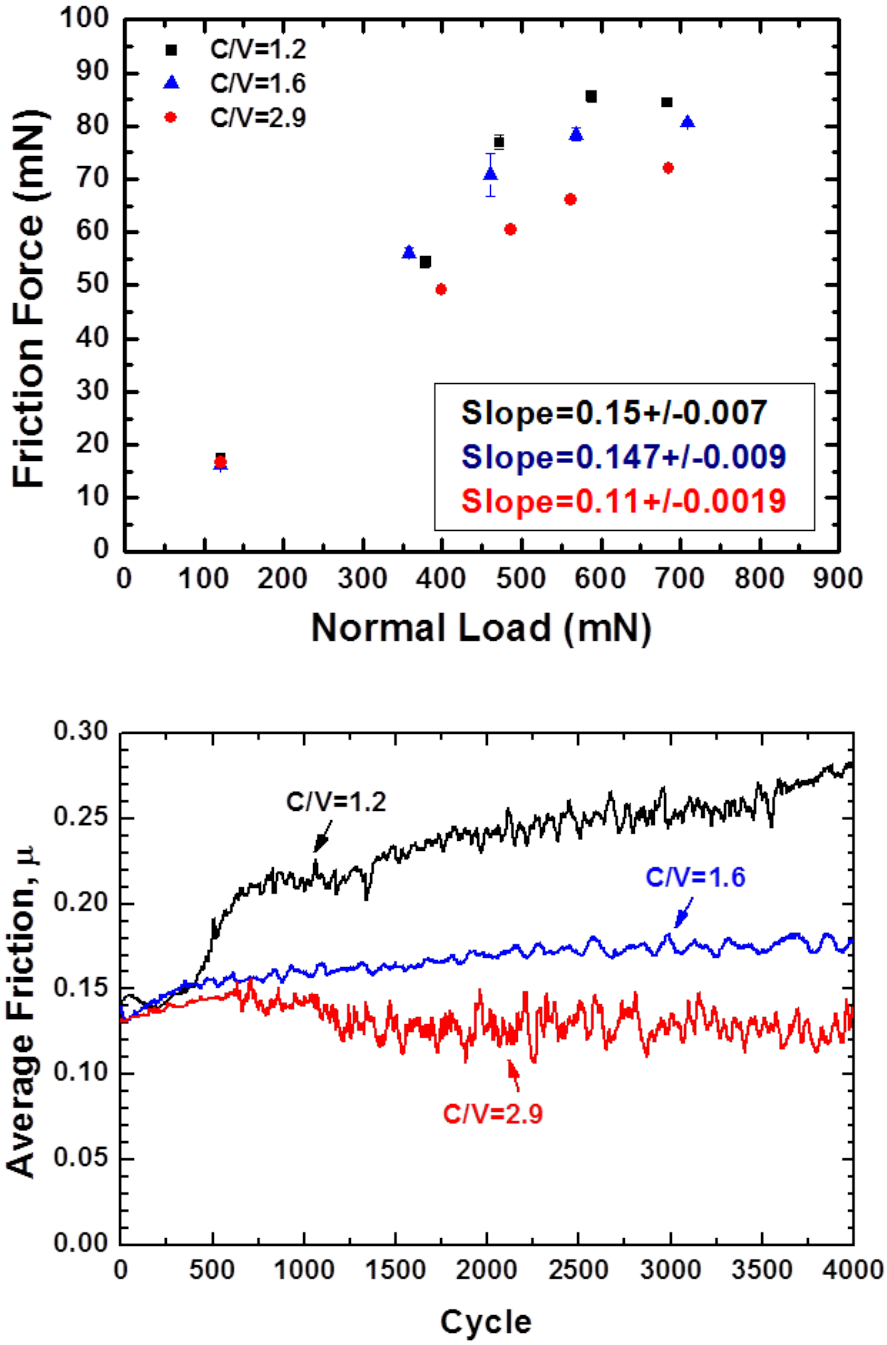

Figure 6 (a) Friction vs. Normal Load for the various coatings performed using micro-scale sliding contacts. (b) Average coefficient of friction vs. the number of cycles for the microtribology experiments using a normal load of 1 N.

3.2.3 Macro-scale Sliding Experiments

Macro-scale sliding tests are also performed in order to elucidate the performance of these coatings in applications with lager contact areas and normal loads. The results are presented in Figure 7 (a) in terms of the friction coefficient vs. sliding time. The friction is initially similar for the lowest and highest carbon content coatings. Upon further sliding however, the friction increases drastically for the high vanadium coating up to approximately 0.5. Subsequently, the friction coefficient fluctuates between 0.4 and 0.6 for the remainder of the test. The lowest carbon content coating show a different behavior; upon the initial sliding, the friction decreases to approximately 0.2 where it remains relatively steady for the remainder of the test, indicating steady state sliding. The coating with a C/V=1.6 ratio follows the trend of this trend relatively closely with a steady state coefficient of friction slightly above 0.2.

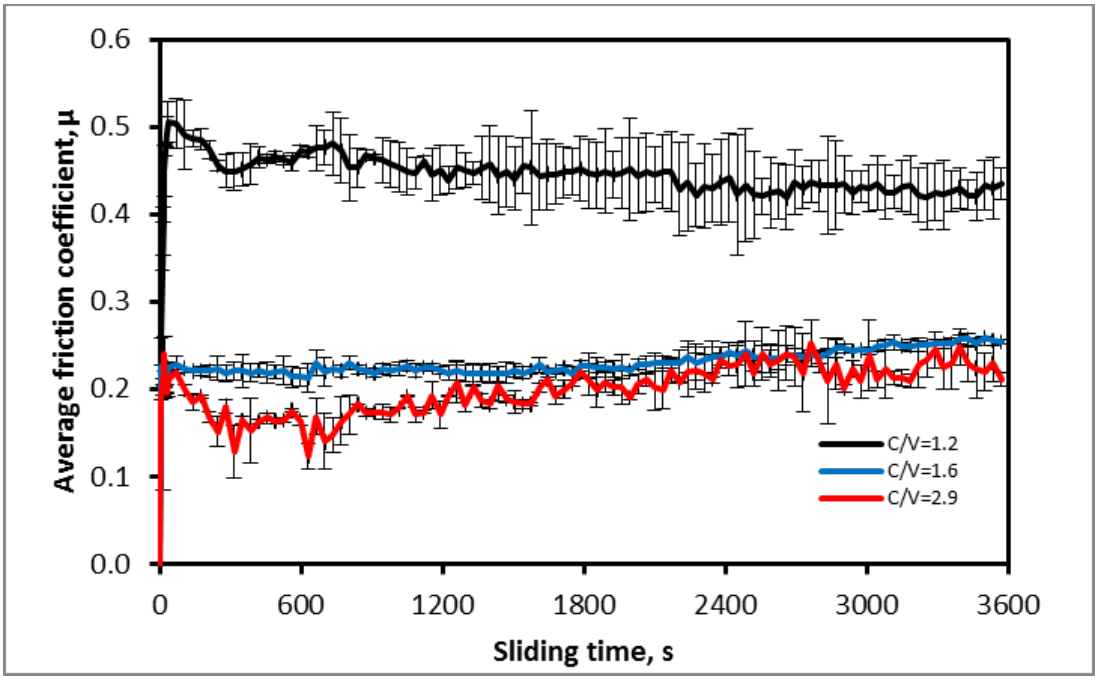

Figure 7 Friction coefficient vs. time for various V-C coatings tested under macroscopic sliding experiments using a sapphire counterface.

A similar behavior to the coefficient of friction is also observed with wear rates for the macro-scale experiments, as shown in Figure 8 (a). The wear rate (i.e. at the end of the experiments) is

nearly an order of magnitude lower for the highest carbon coating compared to the other two coatings. This observation correlates well with the ex situ analysis of the counterfaces; topographical images, shown within the plot, reveal a stable transfer film on the sapphire counterface for the high carbon content coating and no transferfilm for the low carbon content coating. Further analysis of this transferfilm phenomenon and wear track is performed by means of SEM and shown in Figure 8 (b). The transfer film is clearly visible for the coating with the highest C/V. XPS depth profile of the contact region reveals a high carbon concentration ranging between 60 and 40 at.%, as shown in Figure 9. In addition, an oxide concentration between 30 and 40 at.% is observed within the contact region, which is likely in the form of vanadium oxide or aluminum oxide (i.e. material of the counterface).

(a)

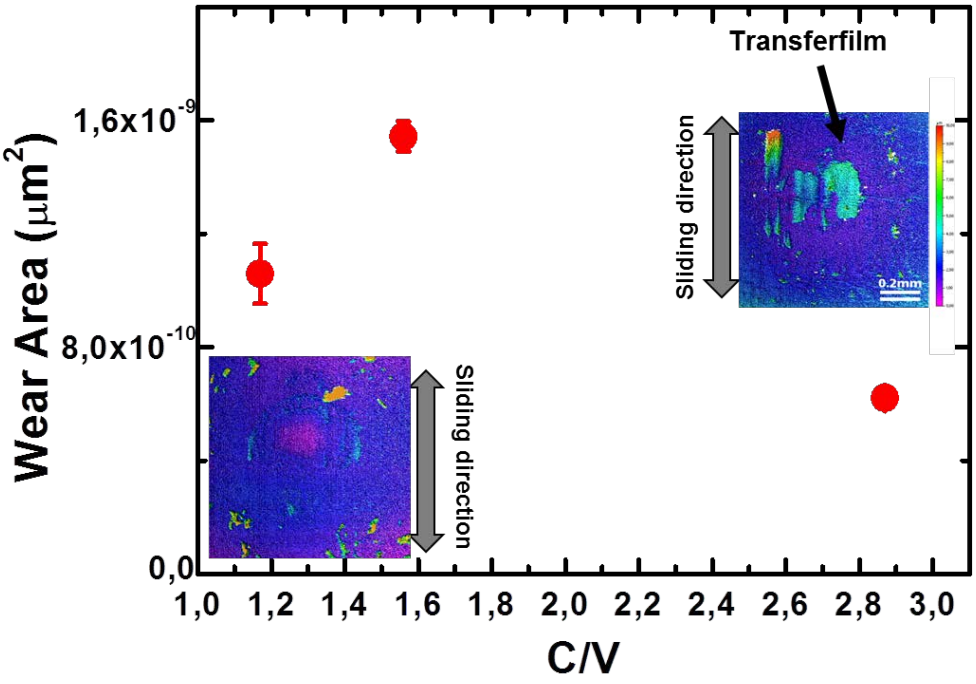

(b)

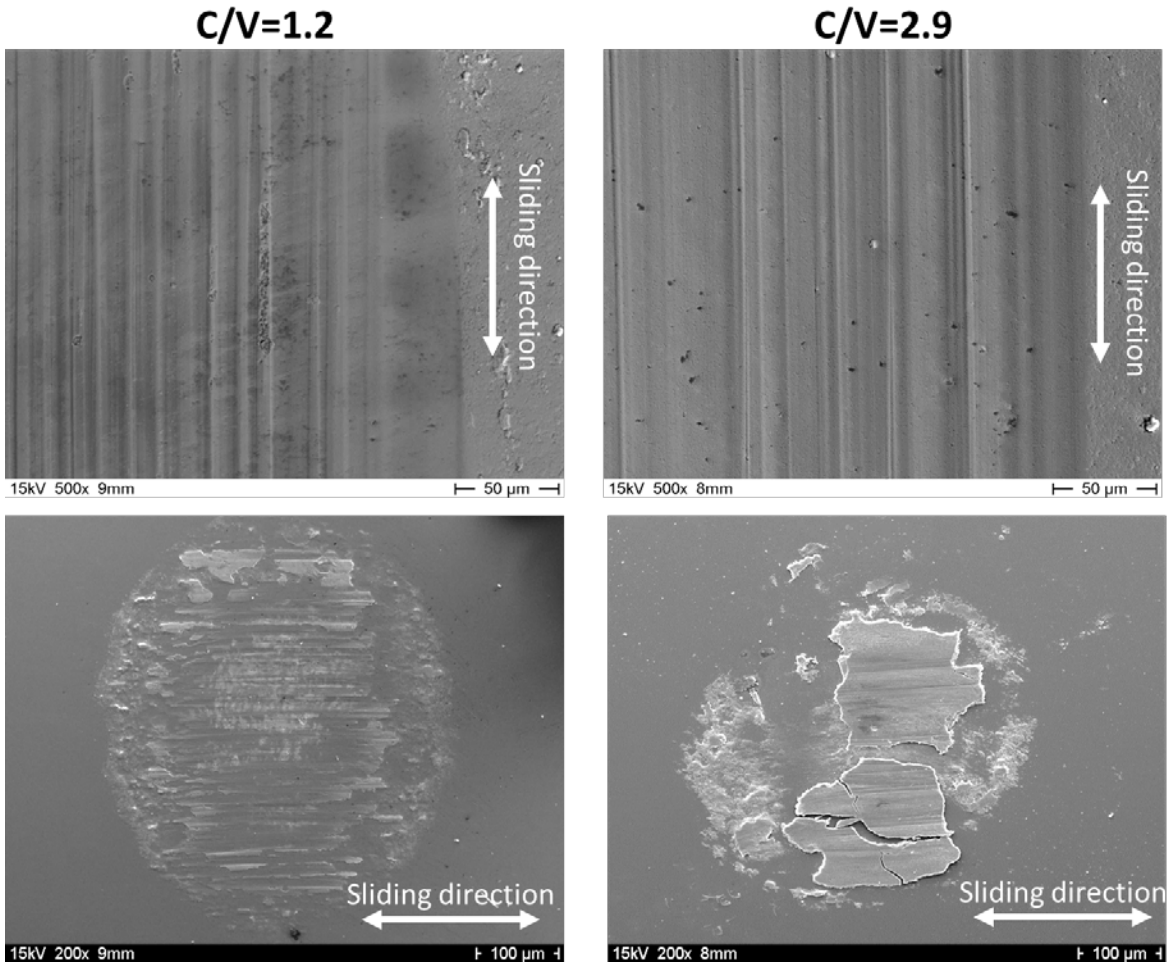

Figure 8 (a) Wear Area vs. C/V ratio and **(b)** SEM images of the wear tracks and worn counterfaces for the coatings with C/V=1.2 and C/V=2.9

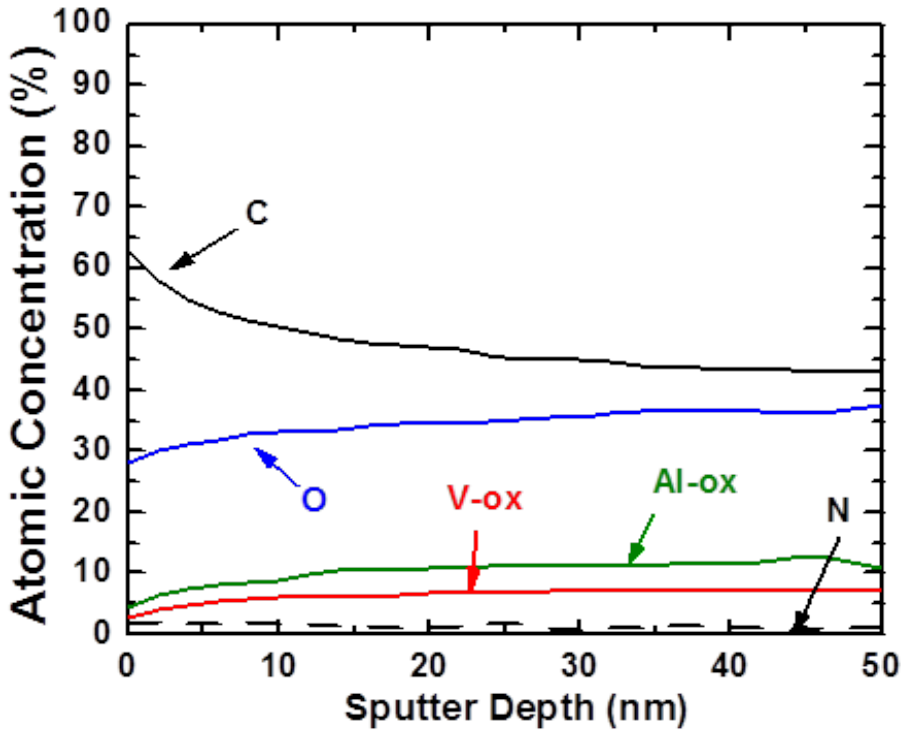

Figure 9 Elemental analysis of the transferfilm in terms of the atomic concentration vs. sputter depth

Further analysis of this third body phenomenon is performed on the worn vanadium carbide surfaces by means of mirco-Raman spectroscopy. The intensities of the D (disordered) and G (graphitic) peaks as a function of the C/V ratio is shown in Figure 10 (a) for the worn and unworn surfaces. While in both cases (i.e. the worn and unworn) the intensities of the G and D peaks increase as a function of the C/V ratio, the intensities of the worn surfaces are noticeably higher compared to the as deposited coatings. In addition, the percent increase in the intensities of the D and G peaks increases with increasing the carbon content (i.e. ~190% and ~350% for the lowest and highest carbon content coating respectively) , as also presented in Table 1. In order to elucidate on the oxide behavior, XPS analysis is performed on the worn surfaces, as

illustrated in Figure 10 (b). Interestingly, nearly no oxygen is detected within the wear track, while a significant amount of oxygen (i.e. high-intensity oxygen peak) is detected within the debris particles surrounding the worn surface.

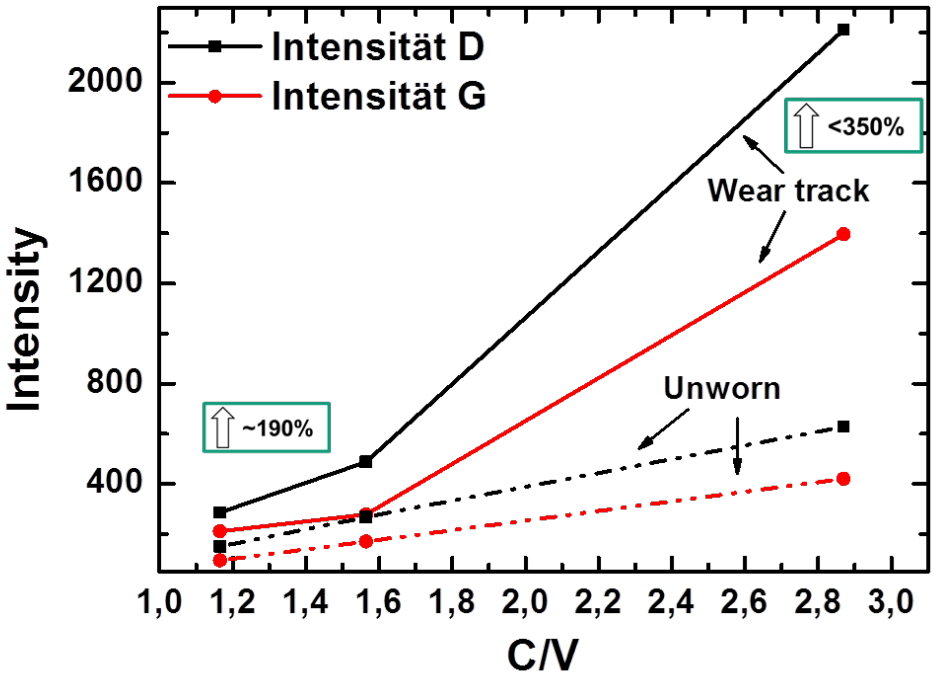

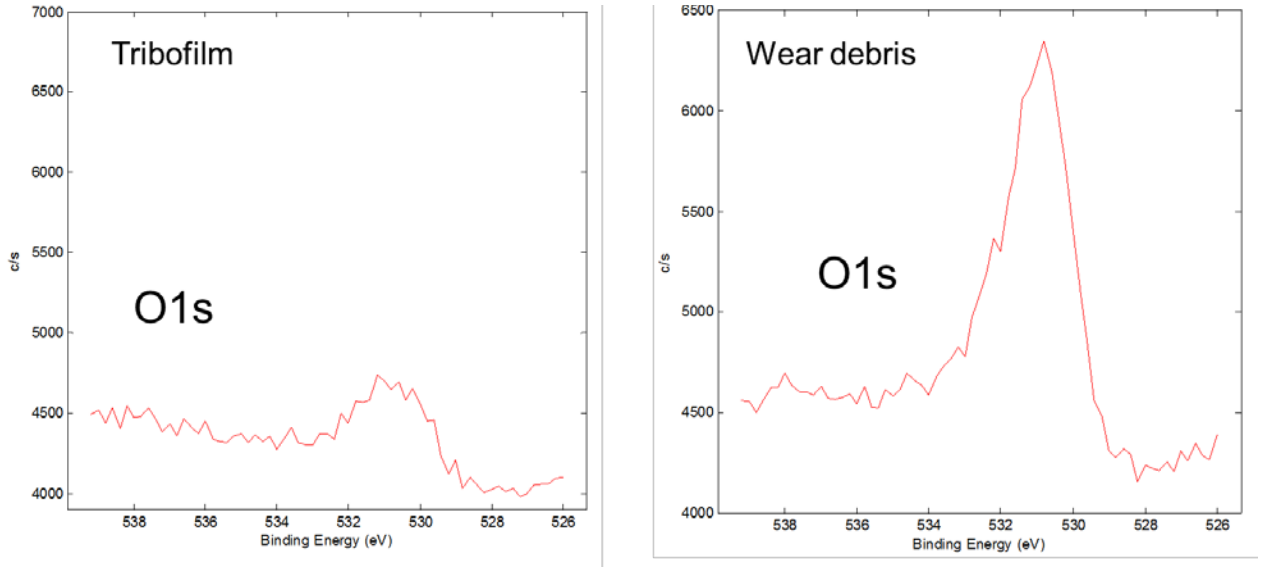

Figure 10 (a) Ex-situ analysis of the V:C wear tracks using micro-Raman spectroscopy and **(b)** schematic representation of the mechanism in a sliding contact leading to a decrease in friction and wear with X-ray photoelectron spectroscopy showing the reduction in oxygen with the wear track and the increase in oxygen within the debris particles.

4. Discussion

In this study, various vanadium carbide based coatings are developed, ranging from single phase nanocrystalline VC_{1+x} to nanocomposite VC/a-C, in order to identify an optimal recipe for tribological applications under unlubricated sliding conditions. The coatings are deposited by means of DC magnetron sputtering and are analyzed in terms of their elemental composition and structure using XPS, micro-Raman, AFM, SEM and XRD. The atomic concentration of the carbon and vanadium observed with the XPS is consistent with the EPMA evaluation, Consequently, the volume fraction of amorphous carbon increases and the crystalline character of the films decreases with increasing the carbon content, as indicated by the XRD analysis. This behavior has been previously observed with similar types of coatings, where the carbon content plays a significant role on the structure of the coating (*9, 75*)

The mechanical properties of the coatings correlate well with the elemental and structural analysis; the hardness and reduced modulus decrease with increasing the carbon content. The decrease in strength with the higher carbon content has previously been observed and is attributed to the amorphous carbon structure (*9, 58, 70*). Wu et al. (*58*) investigated the variation in hardness and modulus with respect to the carbon content in vanadium carbide coatings and showed that the mechanical properties increase up to 50 at.% C and then decrease with further increasing the carbon content. The authors attributed the decrease in the hardness and modulus with the higher carbon content to the higher amount of amorphous carbon. Similarly, Aguzzoli at al.(*70*) observed an increase in hardness until C/V approaches unity and a decrease in hardness for C/V>1, which was explained by the amorphous carbon clusters present in the VC matrix. Indeed, the higher carbon content increases the degree of amorphization and thus the amount of disorder and microscopic defects, as shown with the cross-sectional SEM images and XRD analysis in our study.

The hardness and reduced modulus behavior with respect to the carbon content is consistent with the H^3/E^2 evaluation, which decreases with increasing the C/V ratio. Generally, H^3/E^2 is considered to be a good indicator for the materials resistance to plastic deformation (*71*). Correspondingly, in this study the H^3/E^2 values correlates well with the critical load obtained from scratch tests, where the highest scratch resistance is observed with the highest vanadium content coating. While the H/E and/or H^3/E^2 are simple predictors of the wear resistance, in many tribocouples the continuous sliding contact (e.g. in reciprocating motion) is more complex due to the interfacial processes that govern the friction and wear behavior and thus, these ratios are often not reliable, as previously observed with in situ techniques (*76*).

In order to evaluate the reliability of these coatings in terms of continuous sliding contacts at a wide range of conditions (i.e. normal load and contact area), here we link micro- to macroscopic tribology. The higher carbon content coating reveals the lowest friction and highest wear for the sliding experiments at the micro- and macroscopic length scales, which is opposite to the scratch tests and contradictory to what one would predict based on the hardness and H^3/E^2 values. The inconstancy between the scratch tests and the sliding experiments is attributed to the different nature of the sliding mechanisms resulting in dissimilar interfacial phenomena. Indeed, the continuous reciprocating sliding, inducing higher dissipated energy, higher amount of structural and chemical changes in the near surface regions of both surfaces. For instance, ex situ analysis micro-Raman analysis of the worn surfaces showed an increase in D- and G-peak intensity compared to the unworn surface, indicating the formation of a carbon-rich tribofilm. In addition, the highest increase in intensity is seen with the highest C/V ratio coating, which correlates well with the lower friction and wear values compared to the other coatings. Similarly, a uniform, carbon-rich transferfilm is observed on the counterface sliding against these coatings, while no evident (or stable) transferfilm is observed with the other two coatings. Thus, the sliding of the carbon-transferfilm against the carbon-tribofilm results in low friction and high wear resistance. This phenomenon correlates well with literature on transition-metal carbide materials (*9, 77, 78*), where the high carbon content comprises a self-lubricating phase.

In addition to the tribo- and transferfilm formation, nearly no oxygen is present within the wear track, while the debris particles surrounding the wear track reveled high amount of oxygen. This indicates that the oxygen is removed from the surface during the sliding and is ejected from the

wear track in the form of debris particles surround the wear track or the contact area on the counterface resulting in nearly pure carbon-on-carbon sliding and consequently low friction and wear. This phenomenon is illustrated by the XPS analysis shown in Figure 10 (b).

While the higher carbon content coating reveals the lowest friction and highest wear for the sliding experiments at both length scales (i.e. micro- and macroscopic), the friction values for the microtribology tests are overall lower compared to the macro-scale tests. This observation is somewhat opposite to what one would expect when correlating micro- to macroscale tribology(*79*). In a previous study on MoS_2- based solid lubricants(*79*), the coefficient of friction was lower with micro-scale sliding contacts compared to macrotribology, which was attributed to differences in the velocity accommodation modes (i.e. micro-plowing and plowing events in microscopic contacts). For the vanadium carbide coatings in this study, it is possible that the increase in friction for macroscopic sliding contacts is due to a thicker transfer film, which leads to an additional velocity accommodation mode (i.e. transferfilm shearing) and consequently higher frictional resistance. *In situ* tribometry will be performed on these coatings with video microscopy of the contact in order to verify this assumption and will be presented in a future study.

5. Conclusion

In this study we investigate the influence of C/V ratio (i.e. from pure crystalline VC1-x to nanocomposite VC1-x/a-C thin films) on the microstructure, mechanical properties, and tribological behavior to assess the reliability and limitations of vanadium carbide-based (VC_{1+x}) coatings. In particular, we link micro-to macrotribology in order to provide a better

understanding of the sliding mechanisms of under a wide range of normal loads and contact conditions. The mechanical properties (i.e. hardness (H) and the reduced modulus (Er)) of the coatings decrease with increasing the carbon concentration, which correlates well with the adhesion results obtained from scratch tests. However, reciprocating micro- and macroscale tribological tests reveal higher friction values and increased wear with the high vanadium content coatings. This sliding behavior is attributed to differences in the third body formation and velocity accommodation modes, which are analyzed ex situ by means of XPS, micro-Raman spectroscopy and atomic force microscopy. The coatings with the highest carbon content showed the formation of a uniform, carbon-rich transferfilm on the counterface as well as a carbon-rich tribofilm on the surface of the coating. Consequently, the sliding of the carbon-transferfilm against the carbon-tribofilm results in low friction and high wear resistance.

Acknowledgments

The authors would like to acknowledge the Deutsche Forschungsgemeinschaft for financial support.

References

1. O. Barrau, C. Boher, R. Gras, F. Rezai-Aria, Analysis of the friction and wear behaviour of hot work tool steel for forging. *Wear* **255**, 1444 (2003).
2. C. Choi, A. Groseclose, T. Altan, Estimation of plastic deformation and abrasive wear in warm forging dies. *Journal of Materials Processing Technology* **212**, 1742 (2012).
3. E. Felder, J. L. Montagu, Friction and wear during the hot forging of steels. *Tribology International* **13**, 61 (1980).
4. W. S. Williams, Transition-metal carbides. *Progress in Solid State Chemistry* **6**, 57 (1971).
5. *Transition Metal Carbides and Nitrides*. L. Toth, Ed., (Academic Press, Inc., 1971).
6. S. T. Oyama, in *The Chemistry of Transition Metal Carbides and Nitrides,* S. T. Oyama, Ed. (Springer Netherlands, 1996), pp. 1-27.
7. S. T. Oyama, *The Chemistry of Transitin Metal Carbides and Nitrides*. (Springer, 1996).
8. D. J. Ham, J. S. Lee, Transition metal carbides and nitrides as electrode materials for low temperature fuel cells. *Energies* **2**, 873 (2009).
9. U. Jansson, E. Lewin, Sputter deposition of transition-metal carbide films — A critical review from a chemical perspective. *Thin Solid Films* **536**, 1 (2013).

10. U. Jansson *et al.*, Design of carbide-based nanocomposite thin films by selective alloying. *Surface and Coatings Technology* **206**, 583 (2011).
11. P. K. Wright, E. Trent, *Metal Cutting*. (Butterworth-Heinemann, 2000).
12. J. D. Bolton, M. Redington, Plastic deformation mechanisms in tungsten carbide. *J Mater Sci* **15**, 3150 (1980/12/01, 1980).
13. W. Acchar, U. U. Gomes, W. A. Kaysser, J. Goring, Strength Degradation of a Tungsten Carbide-Cobalt Composite at Elevated Temperatures. *Materials Characterization* **43**, 27 (1999).
14. R. Koc, S. K. Kodambaka, Tungsten carbide (WC) synthesis from novel precursors. *Journal of the European Ceramic Society* **20**, 1859 (2000).
15. P. Stoyanov *et al.*, Experimental and numerical atomistic investigation of the third body formation process in dry tungsten/tungsten-carbide tribo couples. *Tribology Letters* **50**, 67 (2013).
16. P. Stoyanov *et al.*, Friction and wear mechanisms of tungsten-carbon systems: A comparison of dry and lubricated conditions. *ACS Applied Materials & Interfaces*, (2013).
17. L. J. Yang, Wear coefficient of tungsten carbide against hot-work tool steel disc with two different pin settings. *Wear* **257**, 481 (2004).
18. H. Engqvist, S. Ederyd, N. Axén, S. Hogmark, Grooving wear of single-crystal tungsten carbide. *Wear* **230**, 165 (1999).
19. Z. Z. Fang, X. Wang, T. Ryu, K. S. Hwang, H. Y. Sohn, Synthesis, sintering, and mechanical properties of nanocrystalline cemented tungsten carbide – A review. *International Journal of Refractory Metals and Hard Materials* **27**, 288 (2009).
20. K. Jia, T. E. Fischer, B. Gallois, Microstructure, hardness and toughness of nanostructured and conventional WC-Co composites. *Nanostructured Materials* **10**, 875 (1998).
21. S. Hogmark, S. Jacobson, M. Larsson, Design and evaluation of tribological coatings. *Wear* **246**, 20 (2000).
22. P. H. Mayrhofer, C. Mitterer, L. Hultman, H. Clemens, Microstructural design of hard coatings. *Progress in Materials Science* **51**, 1032 (2006).
23. O. Wilhelmsson *et al.*, Design of Nanocomposite Low-Friction Coatings. *Advanced Functional Materials* **17**, 1611 (2007).
24. E. Lewin *et al.*, On the origin of a third spectral component of C1s XPS-spectra for nc-TiC/aC nanocomposite thin films. *Surface and Coatings Technology* **202**, 3563 (2008).
25. M. Stueber *et al.*, Multifunctional nanolaminated PVD coatings in the system Ti–Al–N–C by combination of metastable fcc phases and nanocomposite microstructures. *Surface and Coatings Technology* **200**, 6162 (2006).
26. M. Stueber *et al.*, WEAR STUDIES AND CUTTING TESTS OF Ti–Al–N–C NANOCOMPOSITE COATINGS IN MILLING OPERATIONS–TECHNICAL COMMUNICATION. *Machining Science and Technology* **13**, 122 (2009).
27. A. Erdemir, C. Donnet, Tribology of diamond-like carbon films: recent progress and future prospects. *Journal of Physics D: Applied Physics* **39**, R311 (2006).
28. Y. Liu, A. Erdemir, E. I. Meletis, A study of the wear mechanism of diamond-like carbon films. *Surface and Coatings Technology* **82**, 48 (1996).
29. A. Erdemir, C. Bindal, J. Pagan, P. Wilbur, Characterization of transfer layers on steel surfaces sliding against diamond-like hydrocarbon films in dry nitrogen. *Surface and Coatings Technology* **76–77, Part 2**, 559 (1995).
30. A. Erdemir, O. L. Eryilmaz, G. Fenske, *Synthesis of diamondlike carbon films with superlow friction and wear properties*. (AVS, 2000), vol. 18, pp. 1987-1992.
31. J. Fontaine, C. Donnet, A. Grill, T. LeMogne, Tribochemistry between hydrogen and diamond-like carbon films. *Surface and Coatings Technology* **146–147**, 286 (2001).

32. P. A. Dearnley *et al.*, Coatings tribology drivers for high density plasma technologies. *Surface Engineering* **26**, 80 (2010).
33. P. Gupta, V. Singh, E. Meletis, Tribological behavior of plasma-enhanced CVD aC: H films. Part I: effect of processing parameters. *Tribology International* **37**, 1019 (2004).
34. A. Banerji, S. Bhowmick, A. T. Alpas, High temperature tribological behavior of W containing diamond-like carbon (DLC) coating against titanium alloys. *Surface and Coatings Technology* **241**, 93 (2014).
35. M. Balden *et al.*, Metal-doped carbon films obtained by magnetron sputtering. *Surface and Coatings Technology* **200**, 413 (2005).
36. C. Adelhelm, M. Balden, M. Rinke, M. Stueber, Influence of doping (Ti, V, Zr, W) and annealing on the sp2 carbon structure of amorphous carbon films. *Journal of Applied Physics* **105**, 033522 (2009).
37. H. Dimigen, C.-P. Klages, Microstructure and wear behavior of metal-containing diamond-like coatings. *Surface and Coatings Technology* **49**, 543 (1991).
38. M. Stüber, H. Leiste, S. Ulrich, H. Holleck, D. Schild, Microstructure and properties of low friction TiC□C nanocomposite coatings deposited by magnetron sputtering. *Surface and Coatings Technology* **150**, 218 (2002).
39. J. C. Sánchez-López, D. Martínez-Martínez, C. Lopez-Cartes, A. Fernández, Tribological behaviour of titanium carbide/amorphous carbon nanocomposite coatings: from macro to the micro-scale. *Surface and Coatings Technology* **202**, 4011 (2008).
40. Y. Hu, L. Li, X. Cai, Q. Chen, P. K. Chu, Mechanical and tribological properties of TiC/amorphous hydrogenated carbon composite coatings fabricated by DC magnetron sputtering with and without sample bias. *Diamond and Related Materials* **16**, 181 (2007).
41. Y. Pei, D. Galvan, J. T. M. De Hosson, Nanostructure and properties of TiC/aC: H composite coatings. *Acta Materialia* **53**, 4505 (2005).
42. W. Gulbiński *et al.*, Evaluation of phase, composition, microstructure and properties in TiC/aC: H thin films deposited by magnetron sputtering. *Applied Surface Science* **239**, 302 (2005).
43. D. Martinez-Martinez *et al.*, Tailored synthesis of TiC⁄ aC nanocomposite tribological coatings. *Journal of Vacuum Science & Technology A* **23**, 1732 (2005).
44. M. Wang, K. Schmidt, K. Reichelt, H. Dimigen, H. Hübsch, The properties of titanium-containing amorphous hydrogenated carbon films. *Surface and Coatings Technology* **47**, 691 (1991).
45. A. El Mel *et al.*, Titanium carbide/carbon nanocomposite hard coatings: A comparative study between various chemical analysis tools. *Surface and Coatings Technology* **256**, 41 (2014).
46. V. Derflinger, H. Brändle, H. Zimmermann, New hard/lubricant coating for dry machining. *Surface and Coatings Technology* **113**, 286 (1999).
47. M. Abad, M. Muñoz-Márquez, S. El Mrabet, A. Justo, J. C. Sánchez-López, Tailored synthesis of nanostructured WC/aC coatings by dual magnetron sputtering. *Surface and Coatings Technology* **204**, 3490 (2010).
48. N. Carvalho, J. T. M. DeHosson, Microstructure investigation of magnetron sputtered WC/C coatings deposited on steel substrates. *Thin Solid Films* **388**, 150 (2001).
49. K. Bewilogua, R. Wittorf, H. Thomsen, M. Weber, DLC based coatings prepared by reactive dc magnetron sputtering. *Thin Solid Films* **447**, 142 (2004).
50. G. Gassner, P. Mayrhofer, C. Mitterer, J. Kiefer, Structure–property relations in Cr–C/aC: H coatings deposited by reactive magnetron sputtering. *Surface and Coatings Technology* **200**, 1147 (2005).
51. L. Yate, L. Martínez-de-Olcoz, J. Esteve, A. Lousa, Effect of the bias voltage on the structure of nc-CrC/aC: H coatings with high carbon content. *Surface and Coatings Technology* **206**, 2877 (2012).

52. N. Nedfors *et al.*, Structural, mechanical and electrical-contact properties of nanocrystalline-NbC/amorphous-C coatings deposited by magnetron sputtering. *Surface and Coatings Technology* **206**, 354 (2011).
53. R. D. Evans, J. Y. Howe, J. Bentley, G. L. Doll, J. T. Glass, Influence of deposition parameters on the composition and structure of reactively sputtered nanocomposite TaC/aC: H thin films. *Journal of Materials Research* **20**, 2583 (2005).
54. V. N. Lipatnikov *et al.*, Effects of vacancy ordering on structure and properties of vanadium carbide. *Journal of Alloys and Compounds* **261**, 192 (1997).
55. L. Wu *et al.*, Understanding the mechanical properties of vanadium carbides: Nano-indentation measurement and first-principles calculations. *Journal of Alloys and Compounds* **548**, 60 (2013).
56. R. Franz, C. Mitterer, Vanadium containing self-adaptive low-friction hard coatings for high-temperature applications: A review. *Surface and Coatings Technology* **228**, 1 (2013).
57. A. Aouni, P. Weisbecker, T. H. Loi, E. Bauer-Grosse, Search for new materials in sputtered V 1− x C x films. *Thin Solid Films* **469**, 315 (2004).
58. X. Wu, G. Li, Y. Chen, G. Li, Microstructure and mechanical properties of vanadium carbide coatings synthesized by reactive magnetron sputtering. *International Journal of Refractory Metals and Hard Materials* **27**, 611 (2009).
59. M. Kaufholz *et al.*, Monitoring the thin film formation during sputter deposition of vanadium carbide. *Journal of synchrotron radiation* **22**, 0 (2015).
60. L. Deutschmann, J. Messelhäuser, H. Suhr, W. A. Herrmann, P. Härter, Plasma enhanced chemical vapor deposition of vanadium carbide VC1−x and VOx from vanadocene Cp2V. *Advanced Materials* **6**, 392 (1994).
61. M. Aghaie-Khafri, F. Fazlalipour, Vanadium carbide coatings on die steel deposited by the thermo-reactive diffusion technique. *Journal of Physics and Chemistry of Solids* **69**, 2465 (2008).
62. X. S. Fan, Z. G. Yang, C. Zhang, Y. D. Zhang, H. Q. Che, Evaluation of vanadium carbide coatings on AISI H13 obtained by thermo-reactive deposition/diffusion technique. *Surface and Coatings Technology* **205**, 641 (2010).
63. Y. Herrera, I. C. Grigorescu, J. Ramirez, C. Di Rauso, M. H. Staia, Microstructural characterization of vanadium carbide laser clad coatings. *Surface and Coatings Technology* **108–109**, 308 (1998).
64. G. B. Wang, Wear mechanisms in vanadium carbide coated steels. *Wear* **212**, 25 (1997).
65. F. Meunier *et al.*, Synthesis and Characterization of High Specific Surface Area Vanadium Carbide; Application to Catalytic Oxidation. *Journal of Catalysis* **169**, 33 (1997).
66. B. Zhang, Z. Q. Li, Synthesis of vanadium carbide by mechanical alloying. *Journal of Alloys and Compounds* **392**, 183 (2005).
67. J. Ma *et al.*, Low temperature synthesis of vanadium carbide (VC). *Materials Letters* **63**, 905 (2009).
68. R. Kapoor, S. T. Oyama, Synthesis of Vanadium Carbide by Temperature Programmed Reaction. *Journal of Solid State Chemistry* **120**, 320 (1995).
69. J. Laurila, A. Milanti, J. Nurminen, M. Kallio, P. Vuoristo, Microstructure and wear behaviour of a vanadium carbide reinforced weld coating. *Wear* **307**, 142 (2013).
70. C. Aguzzoli, C. A. Figueroa, F. S. de Souza, A. Spinelli, I. J. R. Baumvol, Corrosion and nanomechanical properties of vanadium carbide thin film coatings of tool steel. *Surface and Coatings Technology* **206**, 2725 (2012).
71. A. Leyland, A. Matthews, On the significance of the H/E ratio in wear control: a nanocomposite coating approach to optimised tribological behaviour. *Wear* **246**, 1 (2000).
72. M. Stüber, S. Ulrich, H. Leiste, H. Holleck, Magnetron sputtered nanocrystalline metastable (V, Al)(C, N) hard coatings. *Surface and Coatings Technology* **206**, 610 (2011).

73. M. Stueber, D. Diechle, H. Leiste, S. Ulrich, Synthesis of Al–Cr–O–N thin films in corundum and f.c.c. structure by reactive r.f. magnetron sputtering. *Thin Solid Films* **519**, 4025 (2011).
74. W. C. Oliver, G. M. Pharr, *Journal of Materials Research* **7**, 1564 (1992).
75. A. A. Voevodin, J. P. O'Neill, J. S. Zabinski, Tribological performance and tribochemistry of nanocrystalline WC/amorphous diamond-like carbon composites. *Thin Solid Films* **342**, 194 (1999).
76. H. W. Strauss, R. R. Chromik, S. Hassani, In situ tribology of nanocomposite Ti-Si-C-H coatings prepared by PE-CVD. *Wear* **272**, 16 (2011).
77. M. Lindquist, O. Wilhelmsson, U. Jansson, U. Wiklund, Tribofilm formation and tribological properties of TiC and nanocomposite TiAlC coatings. *Wear* **266**, 379 (2009).
78. D. Martínez-Martínez, C. López-Cartes, A. Fernández, J. C. Sánchez-López, Influence of the microstructure on the mechanical and tribological behavior of TiC/a-C nanocomposite coatings. *Thin Solid Films* **517**, 1662 (2009).
79. P. Stoyanov, H. Strauss, R. R. Chromik, Scaling Effects between Micro- and Macrotribology of Ti-MoS_2 Coatings. *Wear* **274-275**, 149 (January, 2012).